

**AFRL-IF-RS-TR-2006-308**  
**Final Technical Report**  
**October 2006**



# **SIMULATION OF BIOMOLECULAR NANOMECHANICAL SYSTEMS**

**Regents of the University of California**

**Sponsored by**  
**Defense Advanced Research Projects Agency**  
**DARPA Order No. K900**

*APPROVED FOR PUBLIC RELEASE; DISTRIBUTION UNLIMITED.*

## **STINFO FINAL REPORT**

The views and conclusions contained in this document are those of the authors and should not be interpreted as necessarily representing the official policies, either expressed or implied, of the Defense Advanced Research Projects Agency or the U.S. Government.

**AIR FORCE RESEARCH LABORATORY**  
**INFORMATION DIRECTORATE**  
**ROME RESEARCH SITE**  
**ROME, NEW YORK**

## NOTICE AND SIGNATURE PAGE

Using Government drawings, specifications, or other data included in this document for any purpose other than Government procurement does not in any way obligate the U.S. Government. The fact that the Government formulated or supplied the drawings, specifications, or other data does not license the holder or any other person or corporation; or convey any rights or permission to manufacture, use, or sell any patented invention that may relate to them.

This report was cleared for public release by the Air Force Research Laboratory Rome Research Site Public Affairs Office and is available to the general public, including foreign nationals. Copies may be obtained from the Defense Technical Information Center (DTIC) (<http://www.dtic.mil>).

AFRL-IF-RS-TR-2006-308 HAS BEEN REVIEWED AND IS APPROVED FOR PUBLICATION IN ACCORDANCE WITH ASSIGNED DISTRIBUTION STATEMENT.

FOR THE DIRECTOR:

/s/

CLARE D. THIEM  
Work Unit Manager

/s/

JAMES A. COLLINS, Deputy Chief  
Advanced Computing Division  
Information Directorate

This report is published in the interest of scientific and technical information exchange, and its publication does not constitute the Government's approval or disapproval of its ideas or findings.

<b>REPORT DOCUMENTATION PAGE</b>				<i>Form Approved</i> <b>OMB No. 0704-0188</b>	
<small>Public reporting burden for this collection of information is estimated to average 1 hour per response, including the time for reviewing instructions, searching data sources, gathering and maintaining the data needed, and completing and reviewing the collection of information. Send comments regarding this burden estimate or any other aspect of this collection of information, including suggestions for reducing this burden to Washington Headquarters Service, Directorate for Information Operations and Reports, 1215 Jefferson Davis Highway, Suite 1204, Arlington, VA 22202-4302, and to the Office of Management and Budget, Paperwork Reduction Project (0704-0188) Washington, DC 20503.</small>					
<b>PLEASE DO NOT RETURN YOUR FORM TO THE ABOVE ADDRESS.</b>					
<b>1. REPORT DATE (DD-MM-YYYY)</b> OCT 2006		<b>2. REPORT TYPE</b> Final		<b>3. DATES COVERED (From - To)</b> Aug 01 – Dec 05	
<b>4. TITLE AND SUBTITLE</b>  SIMULATION OF BIOMOLECULAR NANOMECHANICAL SYSTEMS (BioNEMS)				<b>5a. CONTRACT NUMBER</b>  	
				<b>5b. GRANT NUMBER</b> F30602-01-2-0540	
				<b>5c. PROGRAM ELEMENT NUMBER</b> 61101E	
<b>6. AUTHOR(S)</b>  Arup K. Chakraborty and Arunava Majumdar				<b>5d. PROJECT NUMBER</b> E117	
				<b>5e. TASK NUMBER</b> 00	
				<b>5f. WORK UNIT NUMBER</b> 69	
<b>7. PERFORMING ORGANIZATION NAME(S) AND ADDRESS(ES)</b> Regents of the University of California Sponsored Projects Office 336 Sproul Hall Berkeley CA 94720				<b>8. PERFORMING ORGANIZATION REPORT NUMBER</b>  	
<b>9. SPONSORING/MONITORING AGENCY NAME(S) AND ADDRESS(ES)</b>  <div style="display: flex; justify-content: space-between;"> <div style="width: 45%;"> DARPA  3701 North Fairfax Drive  Arlington VA 22203-1714 </div> <div style="width: 45%;"> AFRL/IFTC  525 Brooks Rd  Rome NY 13441-4505 </div> </div>				<b>10. SPONSOR/MONITOR'S ACRONYM(S)</b>  	
				<b>11. SPONSORING/MONITORING AGENCY REPORT NUMBER</b> AFRL-IF-RS-TR-2006-308	
<b>12. DISTRIBUTION AVAILABILITY STATEMENT</b> APPROVED FOR PUBLIC RELEASE; DISTRIBUTION UNLIMITED. PA# 06-724					
<b>13. SUPPLEMENTARY NOTES</b>					
<b>14. ABSTRACT</b> This report documents results from the BioNEMS project. Computer simulation methods and theoretical tools that can be applied to guide the design of microdevices relying on the concept of translating biomolecular binding to mechanical forces were developed. These computational tools were applied, in synergy with experiments, to define the important factors that determine device performance. One important result is that molecular-level self assembly of probe molecules determines microdevice performance, and this has had a big impact on the design of cantilever-based microdevices. These findings were used to establish design guidelines and utilized in the fabrication of a prototype device that is being transitioned in to a commercial product. Efforts to translate mechanical signals to electronic ones are also described in this context. New discoveries regarding how T lymphocytes of the immune system detect pathogens can be exploited to create synthetic pathogen detectors that exhibit extraordinary sensitivity and selectivity were examined. Computer simulations exploring T cell signaling were completed as part of this research.					
<b>15. SUBJECT TERMS</b>  Computer simulation, computational tools, biomolecular, binding, self assembly, design, microdevices					
<b>16. SECURITY CLASSIFICATION OF:</b>			<b>17. LIMITATION OF ABSTRACT</b>  UL	<b>18. NUMBER OF PAGES</b>  34	<b>19a. NAME OF RESPONSIBLE PERSON</b> Clare Thiem
a. REPORT U	b. ABSTRACT U	c. THIS PAGE U			<b>19b. TELEPHONE NUMBER (Include area code)</b>

## Table of Contents

List of Figures .....	ii
<b>1.0 Introduction.....</b>	<b>1</b>
<b>2.0 Simulation of Biomolecular Nanomechanical Systems .....</b>	<b>2</b>
Theoretical and Computational Effort .....	2
Nanomechanical forces generated by surface grafted DNA .....	2
Atomistic understanding of DNA hybridization and melting .....	3
Understanding the dynamics of DNA hybridization on cantilevers.....	4
Molecular Dynamics Simulation of Hybridization Kinetics on Cantilevers.....	5
Experimental Effort on Optical Detection .....	6
Microcantilever Array Chip .....	7
Surface Grafting Density of Probe Molecules .....	9
Polymer-Membrane Based Biosensors .....	13
<b>3.0 Electronic Detection on MOSFET-Embedded Microcantilevers .....</b>	<b>16</b>
Simulation of microcantilevers for optimization .....	17
MOSFET Device Fabrication and Testing .....	18
Surface Immobilization of Receptors: .....	20
Electronic Signature of Microcantilever Binding .....	20
<b>4.0 Taking Lessons from T Lymphocyte Biology to Revolutionize Detector Design.....</b>	<b>22</b>
Small amounts of stimulatory pMHC molecules presented on synthetic surfaces stimulate synapse formation .....	23
Single molecule detection of pMHC molecules on supported lipid bilayers and assays of calcium flux .....	24
The effects of molecular crowding on the T cell signaling pathway .....	24
<b>5.0 Summary.....</b>	<b>25</b>
<b>6.0 References.....</b>	<b>25</b>
<b>7.0 Bibliography .....</b>	<b>26</b>
Appendix.....	27

## **List of Figures**

Figure 1:	Illustration of simulation organization for project. ....	1
Figure 2:	Specific biomolecular interactions between target and probe molecules alter intermolecular interactions within a self-assembled monolayer on one side of a cantilever beam. This can produce a sufficiently large surface stress to bend the cantilever beam and generate motion. ....	2
Figure 3:	Calculated cantilever deflection as a function of the grafting density. The effects of disordered adsorption highlighted, for the first time, that molecular level self-assembly controls microdevice performance. ....	3
Figure 4:	Results of atomistic molecular dynamics simulations showing the major routes for base-pair unbinding. Details regarding the free energy changes are described in <sup>6</sup> .....	4
Figure 5:	The predicted dependence of the effective rate of hybridization on grafting density, and comparison with experiment. ....	5
Figure 6:	Potential function used to carry out Molecular Dynamics simulations.....	6
Figure 7:	MD simulations for typical low and high grafting densities. For high grafting densities, bridging is a severe problem.....	6
Figure 8:	Optical and electron micrographs of 5 <sup>th</sup> generation cantilever microarray chip showing the whole chip and a single well. Each chip contains 100 such wells, with each well containing 4-5 cantilevers. All cantilevers in a well are biofunctionalized the same way through fluid inlet. ....	7
Figure 9:	Schematic diagram of the optical readout system based on a beam-deflection technique that utilizes a single laser and a CCD camera to monitor deflections of multiple cantilevers. An actual CCD image of reflection spots from 500 cantilevers is shown. Also shown is the processed image, which identifies the center of mass (COM) of each spot and notes the COM motion for each spot in order to detect the corresponding cantilever deflection. ....	7
Figure 10:	Hybridization Step: Non-complementary DNA was injected into all the wells around 25 minutes and there was only marginal deflection. Complementary DNA was injected to all the wells at 105 minutes and every cantilever started to deflect away from the gold surface. Spikes between the non-complementary and complementary DNA injection were buffer injections. ....	8
Figure 11:	Method to measure surface grafting density of ssDNA onto a gold surface.....	9
Figure 12:	Grafting density of ssDNA measured as a function of ssDNA length and salt concentration. ....	10
Figure 13:	DNA hybridization density and efficiency as a function of DNA length and concentration. The DNA strands are fully complementary in these experiments. ....	10
Figure 14:	DNA hybridization density as function of salt concentration for fully complementary, single base pair mismatch at the proximal 3' end, single base pair mismatch in the middle, and triple base pair mismatches in the middle.....	11
Figure 15:	Grafting density of probe DNA and a hybridization density of target DNA as a function of salt concentration. This can be plotted as hybridization efficiency as a function of grafting density and finally cantilever deflection as a function of hybridization density.....	12
Figure 16:	Measurement of PSA against a background of BSA at 2 mg/ml. ....	12
Figure 17:	Schematic showing p53 peptide on the cantilever, and subsequent phosphorylation by DNA protein kinase. The cantilever deflection and reaction rates are distinctly different when ATP is used as opposed to when ATP analog, or an inhibitor is used.....	13

Figure 18: Binding of analyte species to the probes immobilized on the membrane surface changes the surface stress. The compressive surface stress change as shown in this figure causes an out of plane deflection that increases the air-gap and reduces the capacitance. ....	13
Figure 19: (a) The micro-fabricated sensor chip in comparison with a nickel; chip has a 3X3 array of sensors unit cells; (b) chip with bonded microfluidic cover; (c) unit cell with layout for single ended capacitance measurement; (d) unit cell with layout for differential capacitance measurement; (e) close-up view of the released membrane sensor. ....	14
Figure 20: Normalized capacitance vs. time on (a) toluene and (b) isopropyl alcohol exposure for sensor membranes coated with different thiol molecules. The terminal groups were: MUA -COOH; MUO – OH; DOT – CH <sub>3</sub> .....	14
Figure 21: Adhesive transfer process; (a) uniform adhesive layer on a wafer obtained by spinning, (b) the cover wafer with patterns brought into contact with the adhesive, (c) selective transfer of the adhesive to the cover wafer, (d) the cover wafer aligned with a device wafer, brought into contact and bonded. ....	15
Figure 22: The burst pressure variation with square device. Each point represents one device. Arrows indicate that the bonding did not fail at the indicated pressure. ....	15
Figure 23: Schematic illustration of MOSFET cantilevers approach .....	17
Figure 24: Top view of a Si multilayer cantilever with a 20 $\mu$ m anchor area showing stress distribution. ....	17
Figure 25: SEM image of pair of MOSFET cantilevers, indicating contacts.. ....	18
Figure 26: Noise and S/N data from MOSFET cantilevers .....	19
Figure 27A: MOSFET characteristics for Streptavidin-Biotin binding .....	20
Figure 27B: I <sub>D</sub> versus V <sub>DS</sub> characteristics. ....	21
Figure 28: Schematic illustration of potential of MOSFET-embedded microcantilever array for parallel and multiplexed biomolecular detection.....	22
Figure 29: The synapse, a marker of robust stimulation, forms when a large amount of agonist is used and for a mixture of a small amount of agonist with null pMHC (enhancer). The enhancer, by itself, does not stimulate synapse formation. ....	23
Figure 30: Single molecule imaging shows that roughly 3 molecules of an agonist pMHC displayed on a supported lipid bilayer along with a “sea” of endogenous ligands can be detected. ....	24

## 1.0 Introduction

This report presents work that was performed under the Air Force Research Laboratory's Cooperative Agreement F30602-01-2-0540, entitled, "Simulation of Biomolecular Nanomechanical Systems (BioNEMS)." Funding for this effort came from the Defense Advanced Research Project Agency's Simulation of Biological System (SIMBIOSYS) Program. The work can be broadly classified into three tasks around which the report is organized. In the first task, the goal was to develop computer simulation tools and theoretical analyses that can guide the design of microdevices that sense molecular signatures of potential pathogens by translating biomolecular binding to mechanical signals. A hierarchical approach was adopted involving close synergy between experimental and computational efforts, and models were developed for phenomena that span a spectrum of time and length scales as illustrated in Figure 1 below. The results of this work were then used to establish design guidelines and utilized in the fabrication of a prototype device. The second task was closely related to the first, and aimed to develop methods to detect the signals generated by biomolecular binding using electronics. The third task explored whether new discoveries regarding how T lymphocytes of the immune system detect pathogens can be exploited to create synthetic pathogen detectors that exhibit extraordinary sensitivity and selectivity. This work examined if the extraordinary sensitivity and selectivity of T lymphocytes for antigen could be maintained if the antigen presenting cell was replaced with a synthetic lipid bilayer. Computer simulations exploring T cell signaling were also pursued. The work performed under this effort will be presented by task.

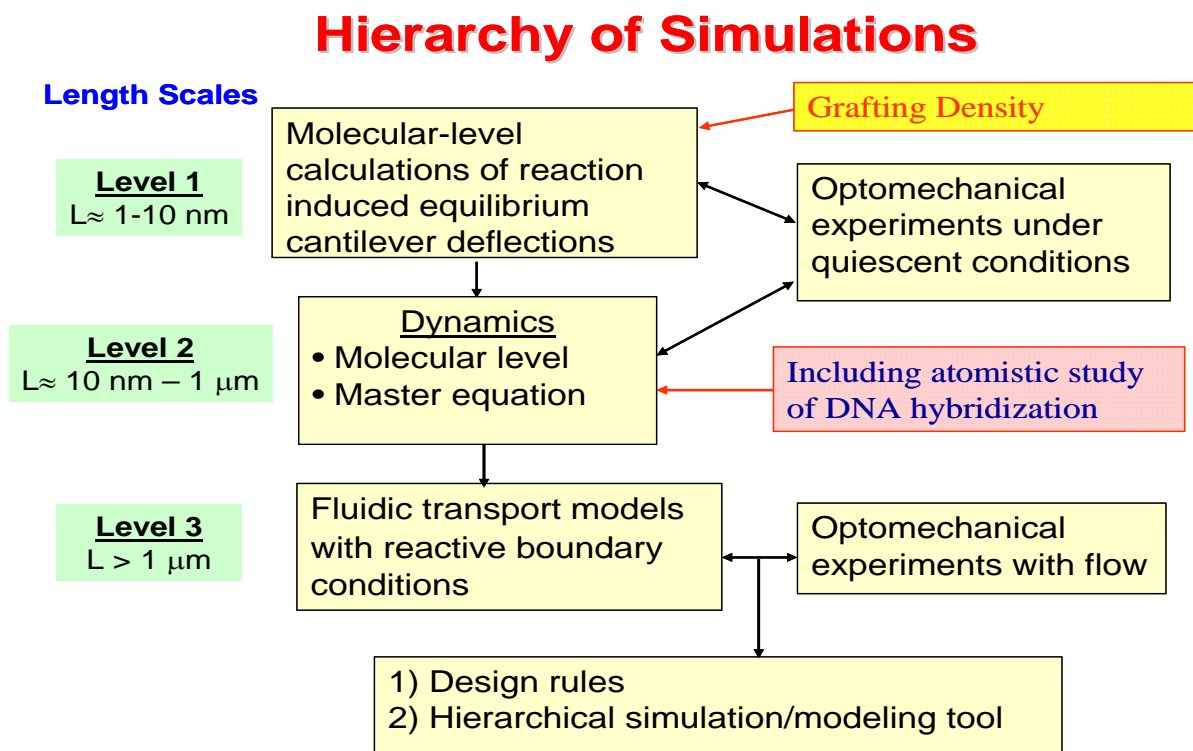


Figure 1. Illustration of simulation organization for project.

## 2.0 Simulation of Biomolecular Nanomechanical Systems

This effort was among the first to show that adsorption of biomolecules on one surface of a microcantilever generates surface stresses that cause the cantilever to deflect, and the adsorption of a second molecule that binds to the bound molecule causes the deflection to change<sup>1,2</sup>. This idea defines the basic platform that was studied (Figure 2). The effect has been demonstrated for various systems<sup>3</sup>. The goal of this project was: (i) to develop simulation methods and design rules that will enable the design of microcantilever-based biosensing systems; and (ii) to develop a prototype microdevice. The project involved synergistic theoretical, computational and experimental work. The outcomes of both the experimental and computational efforts are summarized below.

### Theoretical and Computational Effort

The theoretical and computational work has led to new computational tools. More importantly, the theoretical and computational efforts identified important variables that affect microdesign performance that had not been intuited before and provided design rules that have guided the design of the prototype device whose commercial applications are currently being explored.

This theoretical and computational work led to accomplishments that can be divided into four distinct parts. Each of these is described below.

#### Nanomechanical forces generated by surface grafted DNA

Computational and theoretical tools were first developed that could calculate the deflection of microcantilevers upon adsorption of probe molecules and changes in the deflection upon binding of a target biomolecule to the layer of adsorbed probe molecules. In short, methods were developed that allow us to compute how binding is translated into a mechanical signal, and to understand how various conditions and the identity of the biomolecules influences cantilever deflection. The focus was on DNA hybridization as a prototype system. A model was developed where the free energy contributions due to various effects (e.g., configurational entropy of adsorbed molecules and counterions, hydration energies, etc.) were carefully accounted for. Studies revealed three important points that had not been understood heretofore. First, the dominant contribution to cantilever deflection is hydration forces, not configurational entropy or electrostatics. Secondly, the density with which probe molecules are grafted on to the surface strongly influences cantilever deflection. Thirdly, the cantilever deflection is strongly dependent upon whether or not the grafting of probe molecules on the surface is ordered or is disordered. Disordered distributions, which are most likely in practice, lead to much larger cantilever deflections (Figure 3). These findings highlighted, for the first time, that molecular

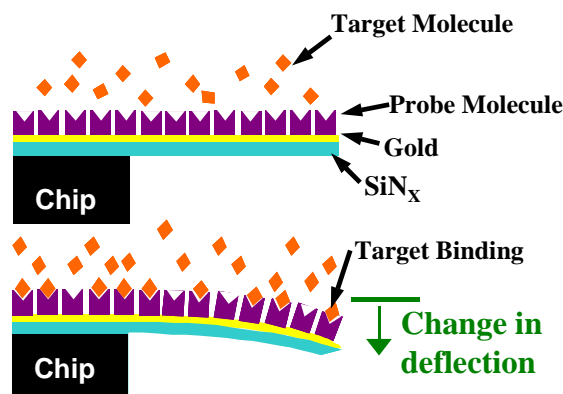


Figure 2. Specific biomolecular interactions between target and probe molecules alter intermolecular interactions within a self-assembled monolayer on one side of a cantilever beam. This can produce a sufficiently large surface stress to bend the cantilever beam and generate motion.



level self-assembly controls the response of the microdevice. This result, and associated scaling relationships were crucial for the experimental program (see below) which ultimately enabled the development of a prototype device. This work is described in detail in an article published in the *J. Physical Chemistry*<sup>4</sup>.

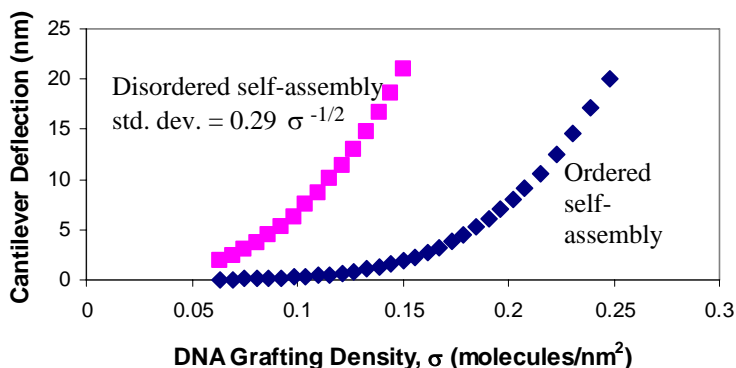


Figure 3. Calculated cantilever deflection as a function of the grafting density. The effects of disordered adsorption highlighted, for the first time, that molecular level self-assembly controls microdevice performance.

### Atomistic understanding of DNA hybridization and melting

In carrying out the work described above, it was discovered that potential functions describing the hybridization dynamics of DNA were not well-developed. The reason for this is that fully atomistic (with explicit solvent) simulations of DNA hybridization had been impossible to carry out because it was computationally intractable to simulate such rare events. A transition path sampling method<sup>5</sup> was applied with the CHARMM (Chemistry at HARvard Macromolecular Mechanics/ program for macromolecular simulations; <http://yuri.harvard.edu>) potential to enable the study of DNA hybridization. This first of its kind study allowed us to determine the molecular pathways of DNA hybridization and melting as well as clarify the role of the solvent in these processes. Figure 4 shows the dominant molecular pathways that were found. This work is significant for two other reasons. First, it provides the basic information necessary for the construction of accurate potential functions for future use. Secondly, the methodology that was developed has now been incorporated in the CHARMM program. This is probably the most commonly used suite of programs used for biomolecular simulations, and so our contribution will help the community at large. This work was been published in the *Proceedings of the National Academy of Sciences*<sup>6</sup>.

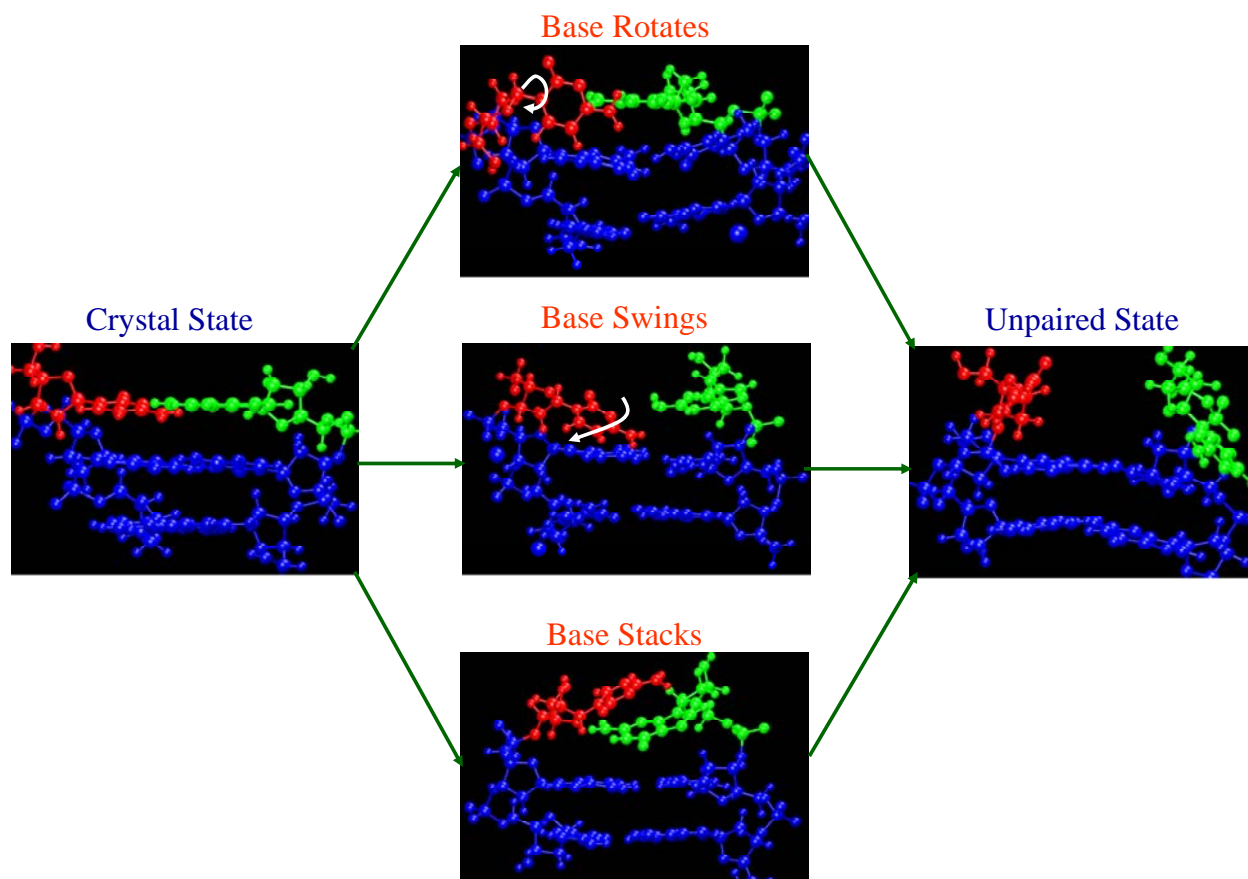


Figure 4. Results of atomistic molecular dynamics simulations showing the major routes for base-pair unbinding. Details regarding the free energy changes are described in<sup>6</sup>.

### Understanding the dynamics of DNA hybridization on cantilevers

In addition to the thermodynamics described above, cantilever deflection is determined by the dynamics of DNA hybridization in an adsorbed layer. Adsorbing the probe molecules on the surface imposes kinetic constraints on the hybridization process that can lead to incomplete binding between target and probe molecules, and this can strongly affect the response of the microdevice. The nucleation of DNA hybridization events depends upon two factors, the probability that complementary regions overlap and the rate of forming a nucleus upon overlap. A stochastic method was developed to investigate how the structure of the adsorbed layer of probe molecules on the cantilever influences the transport of targets on to the layer and subsequent organization of complementary regions leading to nucleation and completion of hybridization. Specifically, Master Equations that can be solved to obtain the stochastic events that describe probe and target molecules in the layer were formulated. These equations were solved to obtain the initial rate of hybridization. For the grafting densities used in the experiments, it was determined that transport of target molecules through the layer is not limiting. Probe-probe and probe-target interactions, however, decrease the number of available nucleation sites. This effect can decrease the effective hybridization rates by over an order of

magnitude even if the intrinsic hybridization kinetics is unchanged from that measured in solution. Higher surface coverages and longer probe lengths exacerbate these effects. Figure 5 shows the effective rate of hybridization as a function of the grafting density of probe molecules. The results are in good agreement with experimentally measured values<sup>6</sup>. Furthermore, in accordance with experiments<sup>7</sup>, we find that targets that preferentially bind to the segments near the grafted end of the probe molecules show more drastic reductions in hybridization rates. This is because nucleation sites near the grafted ends are least accessible. These results suggest that grafting density must be controlled during assembly of the probe

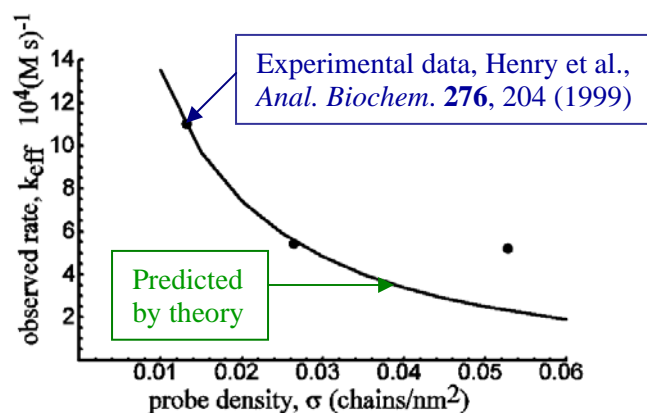


Figure 5. The predicted dependence of the effective rate of hybridization on grafting density, and comparison with experiment.

molecules on the cantilever if reliable microdevice performance is to be obtained. These studies emphasized the importance of the surface chemistry of the cantilever for designing proper microdevices. The results of this theoretical work have been reported in detail in a publication in the *J. Chemical Physics*<sup>8</sup>.

#### Molecular Dynamics Simulation of Hybridization Kinetics on Cantilevers

The weakness of the work described in the preceding subsection is that the Master Equations could only be solved easily to obtain the initial hybridization rates. This is because it was not possible to properly account for changes in the structure of the probe layer during hybridization using this framework. So, to further support these studies emphasizing the importance of grafting density, Molecular Dynamics simulations were carried out. These simulations were carried out using standard molecular dynamics with the potential function shown in Figure 6.

### Molecular dynamics (MD)

Potential: modified bead & spring model

$$V = V_{non-bond} + V_{bond} + V_{angle}$$

$$V_{non-bond}(r) = 4\epsilon \left[ \left( \frac{\sigma}{r} \right)^{12} - \left( \frac{\sigma}{r} \right)^6 \right] r_{cutoff}^b = 2.5\sigma, r_{cutoff} = \sqrt[12]{2}\sigma$$

$$V_{bond}(r) = k_b (r - r_b)^2$$

$$V_{angle}(\theta) = k_\theta (\theta - \theta_0)^2 \times \begin{cases} 0.5(\tanh(8 - r) + 1), & r < r_{cutoff}^b \\ 0, & r > r_{cutoff}^b \end{cases}$$

### Model parameters\*

$$\sigma = 0.53 \text{ nm}$$

$$\epsilon = 1.67 \text{ kcal/mol}$$

$$m = 250 \text{ grams/mol}$$

$$m_{wall} = \infty$$

$$k_b = 6.64 \text{ kcal/(mol A}^2\text{)}$$

$$r_o = 0.34 \text{ nm}$$

$$k_\theta = 42.3 \text{ kcal/mol}$$

$$\theta_o = 180^\circ$$

} all bases

o

\*Numerical values for the model parameters are obtained from DNA X-ray diffraction and bending and stretching experiments described in Ch. 3 and 5 of V. A. Bloomfield, D. M. Crothers, and I. J. Tinoco, *Nucleic Acids: Structures, Properties and Functions* (University Science Books, Sausalito, CA, 2000)

### Simulation details

NVT ensemble; T=300K; PBC;  
 $\rho_g = 0.035\text{-}0.35\text{ chains/nm}^2$ ; one  
 target; each probe/target: 20  
 bps; no solvent;  $10^7$  steps  $\sim \mu\text{s}$

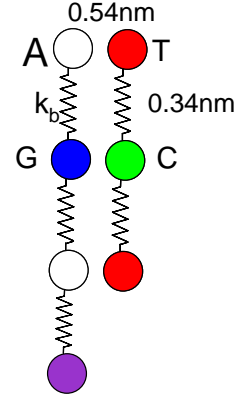
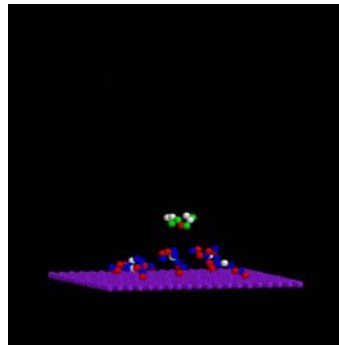
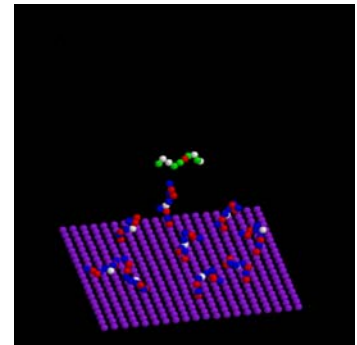


Figure 6. Potential function used to carry out Molecular Dynamics simulations.

The main result is encapsulated in Figure 7 which shows how at larger grafting density hybridization does not occur, but rather, the target chain can bridge across more than one probe molecule. These results also suggested scaling relationships between hybridization efficiency and various parameters that control grafting density (e.g., salt concentration). The results of varying these conditions on grafting density and cantilever deflection are not detailed here because they are reported in the description of the experimental effort (below) as the computational results motivated extensive experiments in this regard (reported in a publication in *Langmuir*<sup>9</sup>).



$$\sigma_g \approx 0.04 \text{ chains/nm}^2$$



$$\sigma_g \approx 0.1 \text{ chains/nm}^2$$

Figure 7. MD simulations for typical low and high grafting densities. For high grafting densities, bridging is a severe problem.

### Experimental Effort on Optical Detection

The experimental effort in this project was originally divided into two components, namely: (i) development of a microcantilever array chip for multiplexed biomolecular analysis; (ii) measurement of surface grafting density of DNA. Both were partially motivated by results

emanating from our computational studies of microcantilever deflection at equilibrium upon DNA hybridization. In addition to these two, another component to the experimental work was added, namely: (iii) development of polymeric membrane based biosensor. Each topic will be discussed in detail now.

### Microcantilever Array Chip

Figure 8 shows a section of the 5<sup>th</sup> generation microcantilever array chip that was developed<sup>10</sup>. This chip contains about 100 wells with each well containing 4-5 cantilevers. There are approximately 500 cantilevers on each chip. Every well has a big I/O for injection of liquid and several small I/O's to prevent bubbles from being trapped inside. The design of the fluidics as well as microcantilever structural characteristics was done in close collaboration with CFDRC researchers<sup>11</sup>. Each cantilever beam is surrounded by its own reaction well which contains two fluidic I/Os.

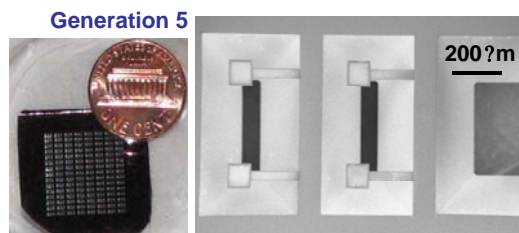


Figure 8. Optical and electron micrographs of 5<sup>th</sup> generation cantilever microarray chip showing the whole chip and a single well. Each chip contains 100 such wells, with each well containing 4-5 cantilevers. All cantilevers in a well are biofunctionalized the same way through fluid inlet.

The microcantilevers were made of SiN<sub>x</sub> and fabricated on a Si wafer, whereas the reaction well is defined on a glass wafer. Each cantilever contains a large paddle for reflecting a laser beam that is used for the optical readout. Figure 9 shows the schematic diagram of the optical readout, where a collimated beam from a low-power HeNe laser (1.5 mW) was expanded and reflected off the whole microarray chip (see Figure 9). The reflected beam from the whole chip was directed towards a CCD (charge-coupled device) camera. Reflection from the paddles appear as spots on the CCD. Because of the initial deflection of the cantilevers, the reflections from the paddles were distinguished from the reflection off the silicon surface. Motion of these CCD spots was monitored to measure the deflections of all the cantilevers simultaneously. Spots from 500 cantilevers were detected and their motion tracked. However, lack of automation of liquid handling and computation power have forced the experiments to be conducted using 40 cantilevers at a time.

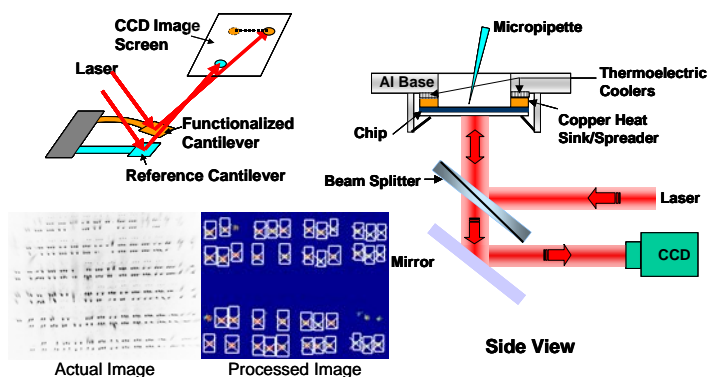


Figure 9. Schematic diagram of the optical readout system based on a beam-deflection technique that utilizes a single laser and a CCD camera to monitor deflections of multiple cantilevers. An actual CCD image of reflection spots from 500 cantilevers is shown. Also shown is the processed image, which identifies the center of mass (COM) of each spot and notes the COM motion for each spot in order to detect the corresponding cantilever deflection.

Figure 10 shows plots of 30 cantilever experiments performed almost simultaneously (within 40 minutes) in 8 wells. Figure 10 shows cantilever deflection as a function of time for DNA hybridization. First, non-complementary target ssDNA 20nt (nucleotide) in length was injected into

all the wells at about 25 minutes. This resulted in no significant cantilever deflections. Complementary target ssDNA 20nt in length was then introduced at 105 minutes in all the wells. The cantilevers immediately responded and produced almost similar levels of deflections. In all cases, the deflections were downward away from the gold surface. In all cases, the cantilever response was observed within 20-30 minutes, which is much shorter than our previous observations.

#### *Achievements and challenges:*

1. **Multiplexed Experiments:** DNA hybridization experiments were repeated successfully. Drift problems were resolved and the raw data usable, as shown in Figure 10. Intrawell consistency and interwell repeatability was seen.
2. **Automation:** A robotic system was designed and fabricated and used to automatically deliver liquid to the microarray in a precise and quick manner.
3. **Surface Chemistry:** A significant amount of time and effort was devoted to developing and integrating surface chemistry to bind receptor molecules and prevent non-specific binding. The options tried for binding proteins to the gold coated cantilever were: (i) DTSSP-NHS (Dithiobis(sulfosuccinimidylpropionate) - Nance-Horan syndrome) / protein using amine chemistry; (ii) thiol-biotin/streptavidin/biotinylated protein; and (iii) thiol-alkane-NHS/protein using amine chemistry. To reduce non-specific binding, polyethylene glycol (PEG) was attached to the bare nitride cantilever surface using silane chemistry. The pros and cons of these options were evaluated and currently options (i) and (iii) are generally used.
4. The cantilever-based antibody array was used for three types of experiments: (i) quantitative analysis of proteins; (ii) direct detection of pathogens such as E. coli by antigen-antibody binding to a membrane protein; and (iii) quantitative analysis of enzyme activity. Preliminary results in both experiments, including controls, were positive.

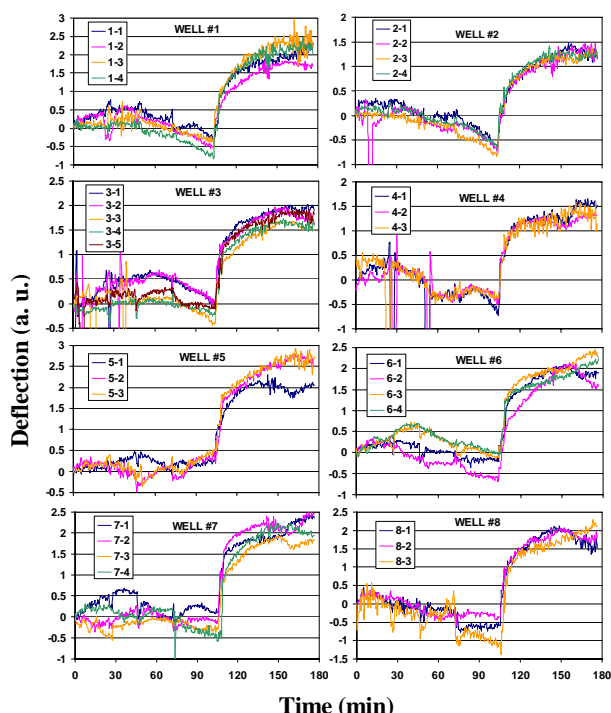


Figure 10. Hybridization Step: Non-complementary DNA was injected into all the wells around 25 minutes and there was only marginal deflection. Complementary DNA was injected to all the wells at 105 minutes and every cantilever started to deflect away from the gold surface. Spikes between the non-complementary and complementary DNA injection were buffer injections.



## Surface Grafting Density of Probe Molecules

### *Measurement Technique and DNA Measurements*

The effort to measure ssDNA surface grafting density was in direct response to the theoretical effort which showed that cantilever deflections depend exponentially on grafting density. This was not known before the beginning of this project. The technique shown in Figure 11 was used. Fluorescently-labeled single-stranded DNA (ssDNA) were first grafted onto a Au-coated surface. They are then reacted with alkane thiols, which competitively bind with the Au surface and remove the ssDNA into solution. The concentration of ssDNA in solution was measured either through UV absorption or through fluorescence. By measuring the ssDNA concentration in solution, fluorescence quenching by gold and fluorescence coupling between neighboring ssDNA were eliminated.

A mercury lamp was used for excitation and a slow-scan CCD camera for detection of fluorescence. The experiments for different DNA lengths and salt concentrations were repeated

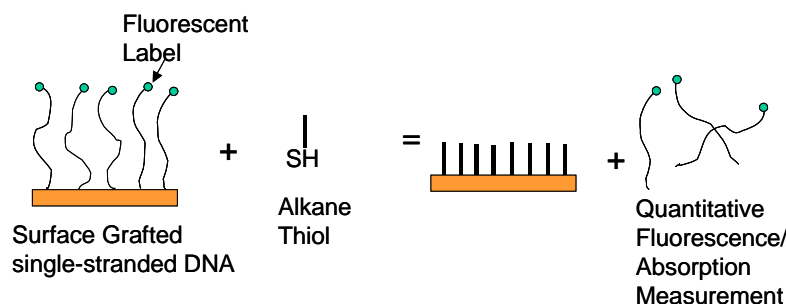


Figure 11. Method to measure surface grafting density of ssDNA onto a gold surface.

and the results are shown in Figure 12. These results correspond well to the results obtained earlier using the laser-photodiode approach. Previous experiments indicated that the interesting range of salt concentrations in which the grafting density changes appreciably lies from 10-100 mM and therefore the research focussed on this range of concentrations. The results of this work was published in a paper that appeared in *Langmuir*<sup>12</sup>.

### *Grafting Density of Proteins on Gold Chips*

An effort in measuring the grafting density of antibodies on a surface was completed<sup>12</sup>. The surface density of anti-PSA (prostate-specific antigen) on gold was determined using the same fluorescence techniques described earlier. The protein was attached to the gold surface using a hetero-bifunctional crosslinker (DTSSP). The immobilized protein was then displaced into solution by adding mercapto-ethanol, which displaces the DTSSP. Finally, the displaced protein in solution was quantitated using the CCD camera and calibrated against a set of protein solutions of known concentrations. The surface density of the immobilized antibody was computed as  $0.0055 \text{ nm}^{-2}$ , which roughly corresponds to about 25% surface coverage assuming a typical size of an IgG (immunoglobulin) molecule.

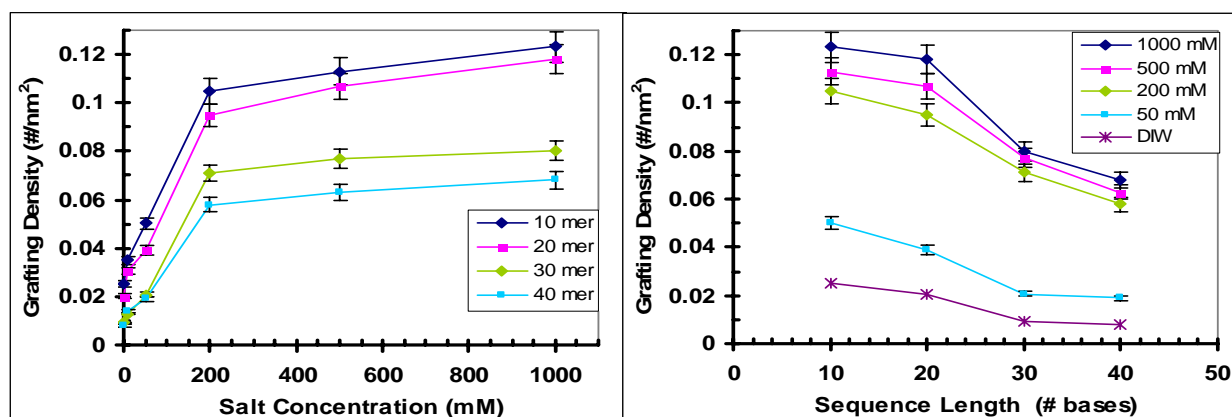


Figure 12. Grafting density of ssDNA measured as a function of ssDNA length and salt concentration.

### DNA Hybridization Efficiency

Based on the discussions at a SIMBIOSYS Principal Investigator's Meeting (Sept. 2003 in Monterrey, CA), experiments were performed using the above-mentioned approach to study DNA hybridization efficiency as a function of DNA length, salt concentration and base-pair mismatches. The data in Figure 13 shows that efficiency decreases dramatically with increasing salt concentration, presumably because of molecular crowding (increasing grafting density –

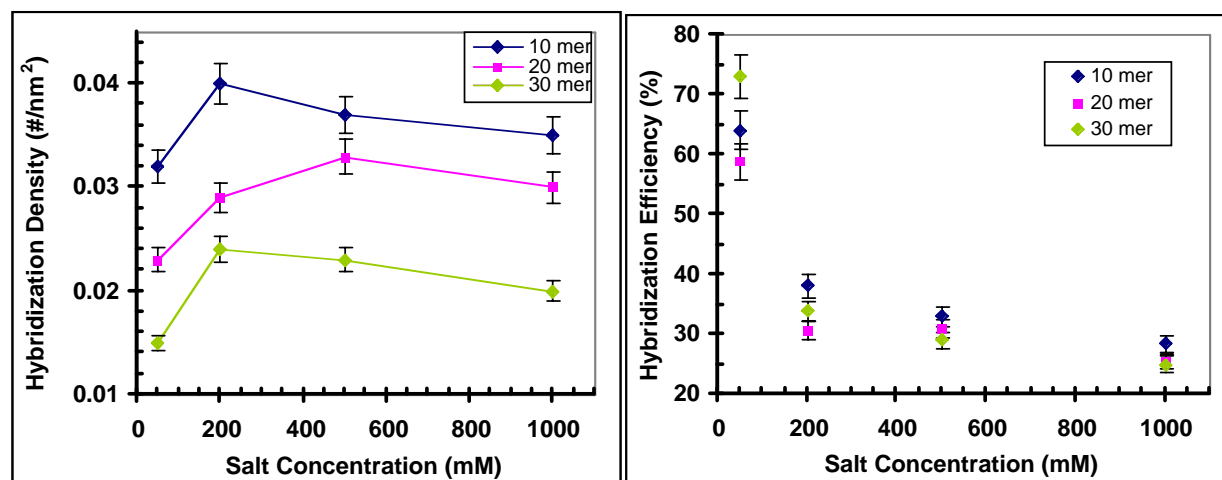


Figure 13. DNA hybridization density and efficiency as a function of DNA length and concentration. The DNA strands are fully complementary in these experiments.

Figure 12). However, increasing grafting density and decreasing hybridization efficiency almost cancel each other producing an almost constant hybridization density. Figure 14 shows the data for hybridization density as a function of base pair mismatches. The data suggests that mismatches at the ends do not alter density, while those in the middle have a marked effect.



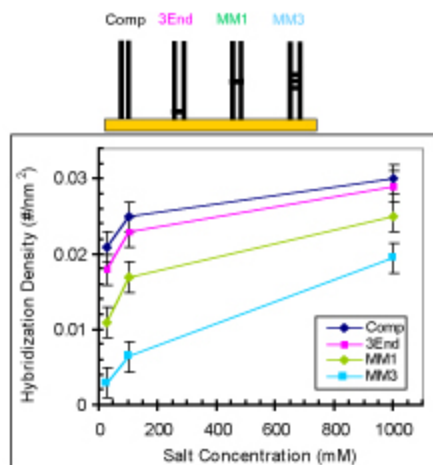


Figure 14. DNA hybridization density as function of salt concentration for fully complementary, single base pair mismatch at the proximal 3' end, single base pair mismatch in the middle, and triple base pair mismatches in the middle.

### *Antigen-Antibody Binding Efficiency*

Experiments were performed to detect the degree of antigen-antibody binding using fluorescence. The purpose of the experiment was to test the effect of antibody immobilization. Two approaches were used: (i) NHS-SS-Biotin (biotin disulphide N-hydroxysuccinimide ester) /Streptavidin/Biotinylated-AntiPSA bound to PSA; (ii) DTSSP-AntiPSA bound to PSA. For the NHS-SS-Biotin approach, the bound PSA density was found to be  $0.0046 \text{ nm}^{-2}$  whereas for the DTSSP approach, the density was found to be  $0.0065 \text{ nm}^{-2}$ . Since the typical size of IgG is about 5 nm, the binding density suggests a surface coverage of 20-25 %.

The influence of grafting density on the cantilever deflection signal was seen by using the control in grafting density of DNA molecules<sup>9</sup>. Figure 15 shows that a scaling relation can be obtained for cantilever deflection by plotting it as a function of hybridization density.

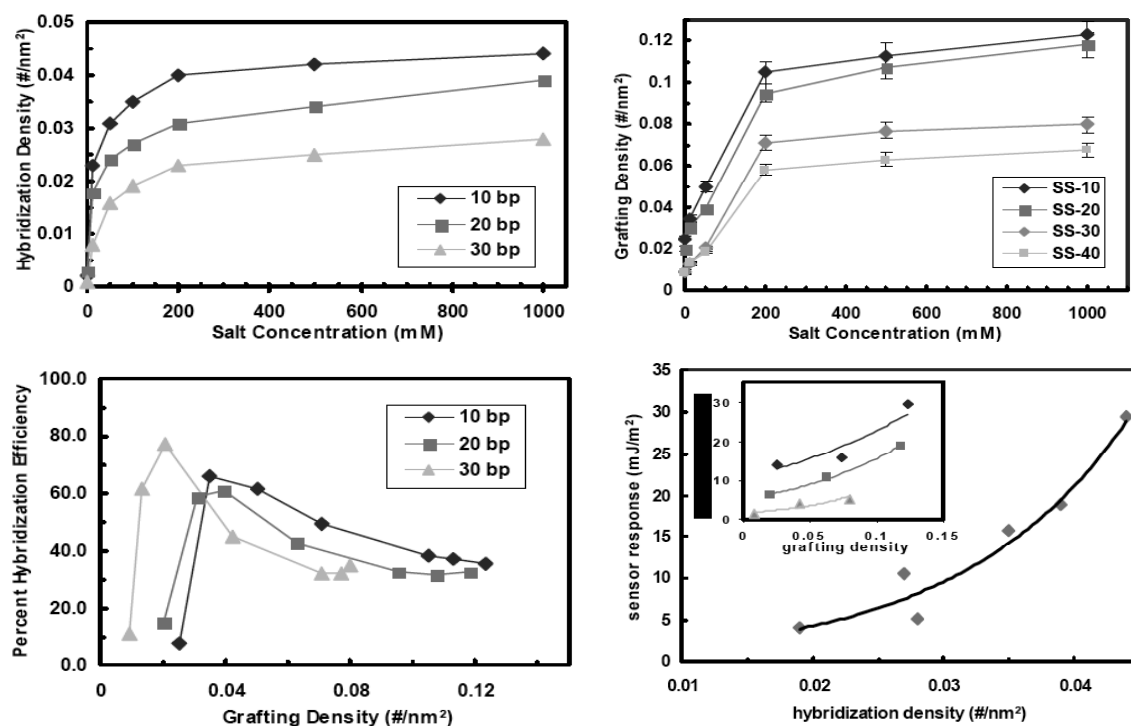


Figure 15. Grafting density of probe DNA and a hybridization density of target DNA as a function of salt concentration. This can be plotted as hybridization efficiency as a function of grafting density and finally cantilever deflection as a function of hybridization density.

Using the surface chemistry that we have developed, we were able to assay at different concentrations. Figure 16 shows our measurement of PSA at concentrations down to 1 ng/ml, against a background of BSA (bovine serum albumin) at 2 mg/ml<sup>13</sup>. We are currently trying to detect such proteins in complex mixtures such as serum.

#### Enzyme Activity

The activity of a kinase during phosphorylation of a serine residue of a peptide attached to a cantilever was detected<sup>13</sup>. Figure 17 shows the schematic.

A monolayer of a peptide from p53 protein containing a recognition element for the DNA protein kinase and serine phosphorylation site was attached to the cantilever using thiol chemistry. Then a DNA protein kinase, along with its reagents, were introduced in the reaction well. The data in Figure 17 suggests that when ATP (adenosine triphosphate) is introduced, the cantilever bends significantly, indicating phosphorylation. This was verified by the experiment

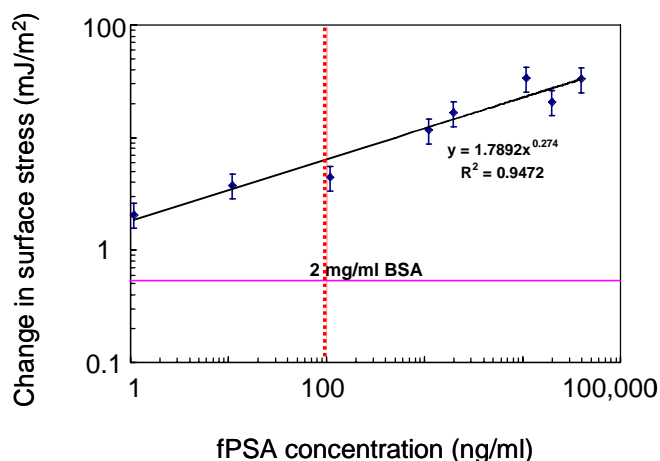


Figure 16. Measurement of PSA against a background of BSA at 2 mg/ml.

with ATP-analog, which cannot be hydrolyzed, which shows no signal. In addition, when a kinase inhibitor was used, there was no signal as well. This clearly proves that phosphorylation

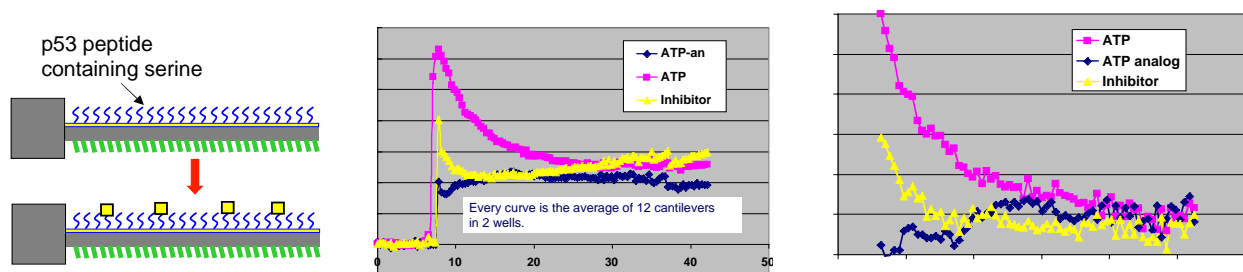


Figure 17. Schematic showing p53 peptide on the cantilever, and subsequent phosphorylation by DNA protein kinase. The cantilever deflection and reaction rates are distinctly different when ATP was used as opposed to when ATP analog, or an inhibitor was used.

can be studied in real time to obtain kinetics.

### Polymer-Membrane Based Biosensors

A new experimental effort that was not part of the original proposal was developed for several reasons:

- (A) The elasticity modulus of polymers is two orders of magnitude lower than most microfabrication materials such as SiNx, Si, etc. This makes the mechanical device more compliant.
- (B) Polymers like parylene are bio-compatible and inert.
- (C) Polymers are hydrophobic, which can allow device design that enables selecting functionalization.
- (D) Easier device fabrication may be possible.
- (E) Membranes are fixed at both ends and hence, may have less drift.

A novel parylene micro-membrane surface stress sensor array using capacitive signal was developed (see Figure 18). This sensor exploits the low elasticity modulus, better chemical resistance and biocompatibility of polymers like parylene when compared to the silicon based materials used in traditional microfabrication. The salient features of the sensor are that it: (i) is label free; (ii) is a universal platform – suitable for both chemical and biological sensing; (iii) uses electronic (capacitive detection) readout; (iv) has integrated microfluidics for addressing individual sensors on the chip; (v) is capable

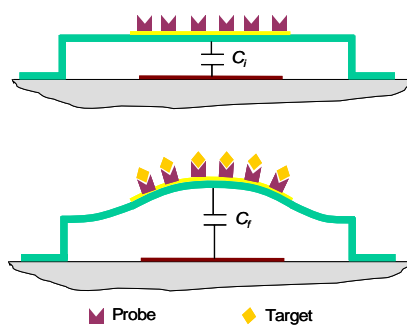


Figure 18. Binding of analyte species to the probes immobilized on the membrane surface changes the surface stress. The compressive surface stress change as shown in this figure causes an out of plane deflection that increases the air-gap and reduces the capacitance.

of handling both liquid and gas samples; (vi) is made using standard low temperature microfabrication processes ( $< 120\text{ }^{\circ}\text{C}$ ); and (vii) can readily be scaled and multiplexed.

Finite element modeling was used for optimization of sensor geometry parameters. A microfabrication process sequence that is compatible with parylene processing was designed using surface and bulk microfabrication techniques to manufacture the prototype of the sensor array. Figure 19 shows optical micrographs of the parylene surface stress sensors with integrated capacitance measurements. This sensor array platform can be tuned for sensing many different targets by using suitable sensor coatings and these coatings play an important role in determining the sensitivity and resolution of the sensor. In the current work, alkanethiols with different functional end groups were chosen as sensor coating materials. Alkanethiol molecules have a strong affinity for gold surfaces and this property was exploited for coating formation on the gold electrodes of the membrane sensor. Furthermore, the use of alkanethiol coating required minimal modification in the sensor microfabrication process sequence.

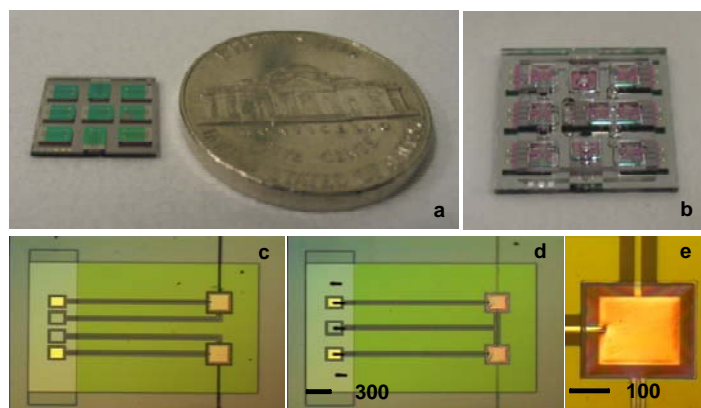


Figure 19. (a) The micro-fabricated sensor chip in comparison with a nickel; chip has a 3X3 array of sensors unit cells; (b) chip with bonded microfluidic cover; (c) unit cell with layout for single ended capacitance measurement; (d) unit cell with layout for differential capacitance measurement; (e) close-up view of the released membrane sensor.

Figure 20 shows the results of multiple functionalized membrane sensors exposed to toluene and isopropyl alcohol. It is clear that the different surface coatings produce different signals. However, the simple alkane thiol molecules do not have selectivity to distinguish between mixtures of gases.

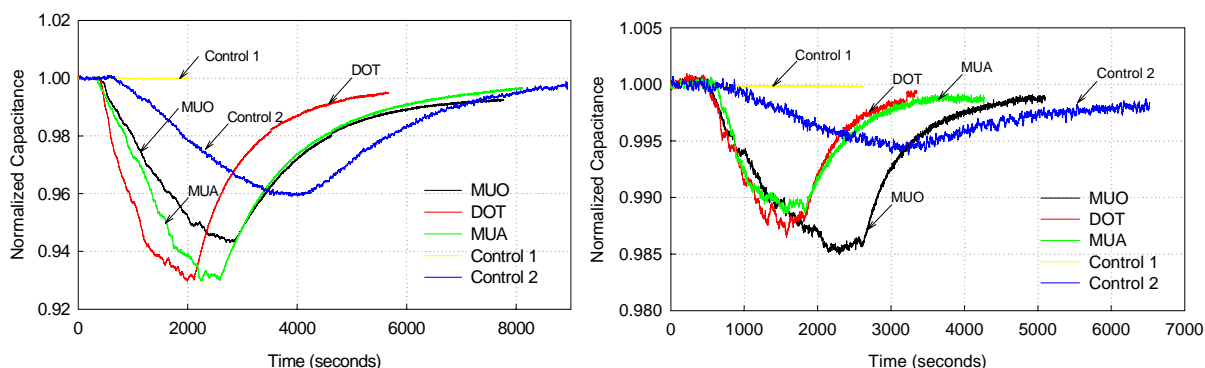


Figure 20. Normalized capacitance vs. time on (a) toluene and (b) isopropyl alcohol exposure for sensor membranes coated with different thiol molecules. The terminal groups were: MUA -COOH; MUO -OH; DOT -CH<sub>3</sub>.

These results now appear in a paper<sup>14</sup> and a PhD thesis<sup>15</sup>.

*The activity under this portion of the research accomplished the following:*

1. Creation of a new electronic method of detecting surface stress using parylene membranes and capacitance detection.
2. Development of a new fabrication process.
3. Concept fabrication and performance testing.
4. Demonstrated chemical sensing using parylene membrane devices.
5. Establishment of a room temperature adhesive bonding process which:
  - a. Designed an experiment for determining the optimum process parameters.
    - Substrates tested: Silicon, Glass, PDMS, Parylene
    - Adhesives: UV curable adhesive, uncured PDMS
    - Burst pressure chosen as device failure criteria.
  - b. Completed the test fixture and test device fabrication.
  - c. Completed a portion of device testing. Microfluidic channels, made by bonding glass and silicon wafers using UV curable adhesives, could withstand 200 psi pressure without leaking.

Figure 21 shows the bonding process while Figure 22 shows the results of burst pressure as a function of size of a square cavity<sup>16</sup>. It is evident that the bonding process can withstand pressure beyond 100 psi, which is adequate for many biofluidic chip applications.

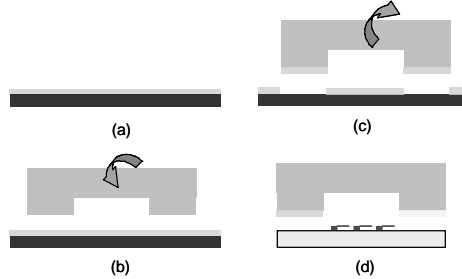


Figure 21. Adhesive transfer process; (a) uniform adhesive layer on a wafer obtained by spinning, (b) the cover wafer with patterns brought into contact with the adhesive, (c) selective transfer of the adhesive to the cover wafer, (d) the cover wafer aligned with a device wafer, brought into contact and bonded.

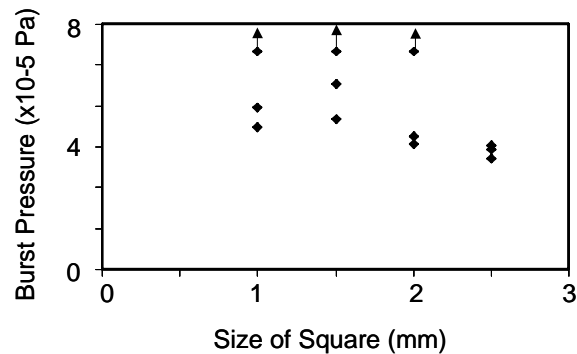


Figure 22. The burst pressure variation with square device. Each point represents one device. Arrows indicate that the bonding did not fail at the indicated pressure.

## Desired performance metrics for microdevice

### *Label-free detection*

- *No reporter molecules; Reduced reagent cost*

*Simultaneous detection of multiple pathogens, molecules, or substances*

*Fast (< 5 min) detection time after sample preparation*

### *Versatile platform for detection*

- *Nucleic acids; antigen-antibody; gas or liquid-based chemicals/toxins*

*Built-in calibration for specific environments*

### *High specificity and sensitivity*

- *Presence or absence of 75bp (base pairs) DNA sequence*
- *Ideally 10fg of DNA from viruses and 100fg (femtogram) of DNA from bacteria*

*Hand-held battery-operated device*

## Commercialization and Technology Transfer

Based on the technology developed under this program, a new company, Kalinex Inc, was launched to commercialize this technology for chemical and biological sensing. Kalinex received a small seedling from DARPA and has also raised private investment from individuals and venture capital. Kalinex currently employs three full time employees and three consultants, and is in the process of making a commercial product for homeland security and industrial applications. Kalinex has also received the option to exclusively license the patents that were filed by UC Berkeley (see Appendix) based on the research conducted under this program. Kalinex is holding discussions with private companies as well as with Transportation Security Agency for launching this product.

### **3.0 Electronic Detection on MOSFET-Embedded Microcantilevers**

The objective of this task was to develop an electronic detection concept for integrated remotely-addressable bio-chem sensors, based on MOSFET-embedded microcantilevers. The task successfully demonstrated the core objective and validated with peer-reviewed archival publications. The research also resulted in intellectual property (IP) related to MOSFET sensing approach, and a patent application has been filed on behalf of Northwestern University (NU).

The specific project goals and research objectives include:

- 1) Simulation of microcantilevers to optimize high surface stress region,
- 2) Design and layout of MOSFET-embedded microcantilevers for biomolecular detection,
- 3) Fabrication of prototype MOSFET on cantilever, and preliminary testing for performance evaluation

The project approach is schematically presented in Figure 23.

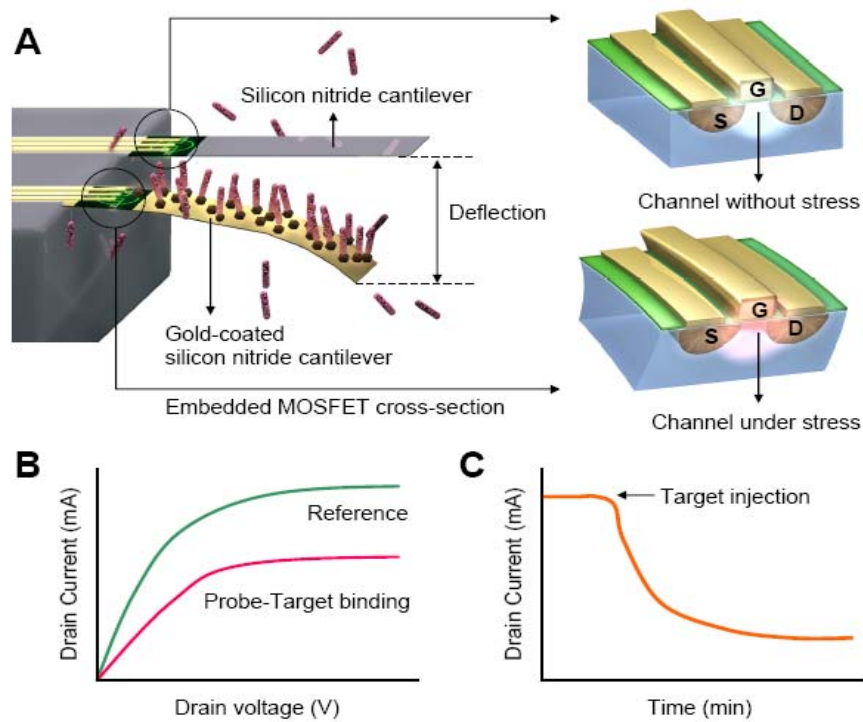


Figure 23. Schematic illustration of MOSFET cantilevers approach.

## Simulation of Microcantilevers for Optimization

To properly identify the high surface stress region on the cantilever, the mechanical properties were modeled and simulated using ANSYS® and Intellisuite® finite-element analysis software. Both packages are available at NU and have been used by a team of experienced microelectromechanical systems (MEMS) researchers for cantilever devices. Solid models of the cantilevers were constructed and proper mesh strategies were determined to simulate cantilever performance (e.g., Figure 24).

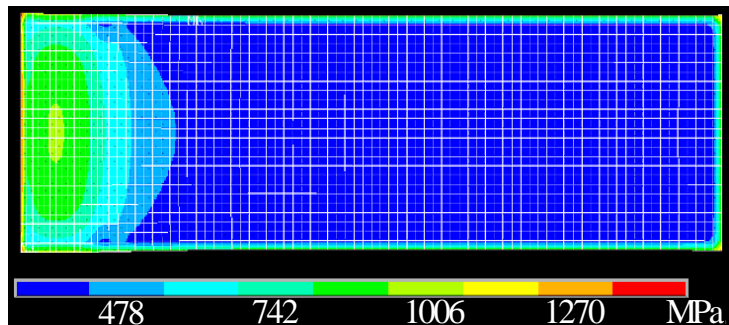


Figure 24. Top view of a Si multilayer cantilever with a 20μm anchor area showing stress distribution.

Optimization of cantilever width, thickness and resonance frequencies was carried out with the software packages mentioned above. Specific cantilever designs were targeted to optimize stress localization at the base of the cantilever for subsequent measurement via MOSFET-stress transistors.

In addition, a resonance frequency analysis of various cantilever designs was carried out to analyze and optimize effects of mass loading. The FEA simulations reduce the need to perform detailed experimental optimization of the device characteristics. Numerous simulation using different cantilever geometries and specifications were carried out. The lengths of the cantilevers in our simulations ranged from 200-450  $\mu\text{m}$  and the thickness from 1.5-3.0  $\mu\text{m}$ . The maximum stress was found to be generated at the base of the cantilever. This area is referred to as the stress concentration region (SCR). These simulated results helped us in guiding where to locate MOSFETs on the cantilever.

## MOSFET Device Fabrication and Testing

Layout of the on-chip MOSFET transistor on the cantilever was carried out using L-EDIT design CAD. Seven masks were designed using L-EDIT to accomplish this goal and mask layout using L-EDIT was converted into a pattern generator file using the PG generation system at the University of Illinois at Chicago (UIC) microfabrication facility. Seven masks on quartz glass plates were developed. The liquid cell around the cantilever chip was designed and laid out for testing in liquid environment.

Si cantilever fabrication was carried out on a SOI (silicon on insulator) wafer with a device layer of 10  $\mu\text{m}$ . Standard Si technology processes such as lithography, PECVD (plasma-enhanced chemical vapor deposition), metal deposition, etching, oxidation and diffusion process were carried out to fabricate the micro cantilever with embedded MOSFET on the high stress region of the cantilever. Most of the microfabrication was carried out in the microelectronics laboratory at UIC. Ion-implantation for source and drain were carried out at the CNF (Cornell NanoScale Science & Technology Facility) user facility. Transistors were placed along the longitudinal direction of the cantilever where stress is maximum and a differential approach was used to measure current change as a result of cantilever bending.

Scanning electron microscopy (SEM) image of one pair of identical cantilevers from an initial 50 x 1 microcantilever array is shown in Figure 25. The pair consists of one microcantilever coated with a thin film of Cr/Au for immobilization of probe molecules, typically with thiol chemistry, and the other was uncoated and acted as the reference. The differential drain current between the sensing and the reference microcantilevers, which further minimizes systematic noise and environmental perturbations, forms the basis for the MOSFET electronic detection (see Figure 23). The differential signal can be fed into a CMOS based differential amplifier for electronic readout at the chip level for future

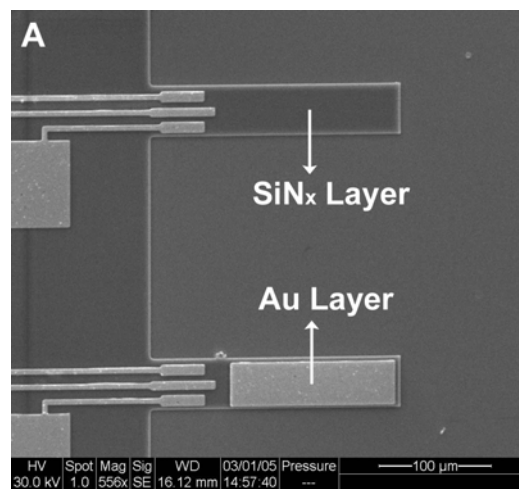


Figure 25. SEM image of pair of MOSFET cantilevers, indicating contacts.



development. MOSFET-embedded micro-cantilevers with the thickness of 1.5 to 2  $\mu\text{m}$  and length ranging from 200 to 300  $\mu\text{m}$  were fabricated, with the separation of about 250  $\mu\text{m}$  between the reference and sensing microcantilevers for simplicity. The transistor was located about 2 to 4  $\mu\text{m}$  from the cantilever base and the W/L ratio of source and drain was around 10 to achieve high transconductance. The resonance frequency of the MOSFET-embedded microcantilevers was around 100 to 150 kHz. Each array was designed to have identical sensor (i.e., Cr/Au-coated) and  $\text{SiN}_x$  reference microcantilevers for differential output to minimize systematic noise and possible false positives. The residual stress that may be introduced by applying a thin layer (30 nm) of gold coating on one side of the cantilever, does not create any notable difference in MOSFET current-voltage characteristics when compared with those of  $\text{Si}_3\text{N}_4$  reference cantilevers.

The drain current sensitivity of MOSFET-embedded microcantilevers to bending was validated using a high-resolution nanomanipulator with <5 nm vertical (Z-axis) resolution. A decrease in drain current between 0.1 to 0.2 mA per nanometer microcantilever deflection was observed. Changes in the drain current by almost one order of magnitude between few to 150 nanometer of microcantilever bending were noted. The bending results indicated that the MOSFET deflection sensitivity was of the same order as optical detection as inferred from the prior literature and almost one-to-two order of magnitude higher than existing active and passive detection technologies.

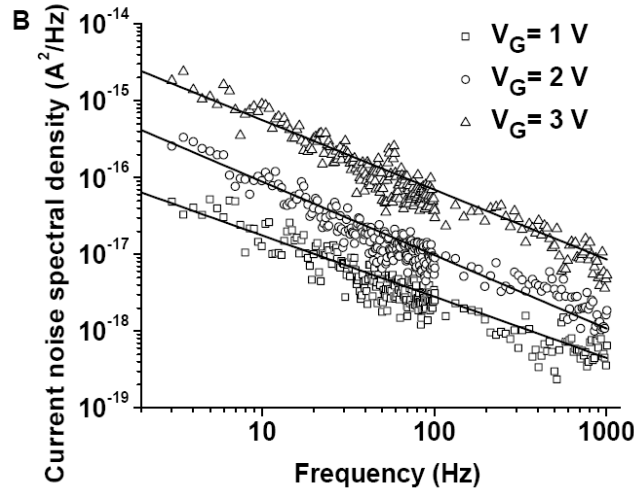


Figure 26. Noise and S/N data from MOSFET cantilevers.

Moreover, MOSFETs have large signal-to-noise (S/N) ratios caused by the large change in drain current relative to the concomitant small noise density in Figure 26. The three curves show  $1/f$  or flicker noise, the dominant source of noise in MOSFETs at low frequencies, at three different voltages (23,24). The current noise of 40-60 nA, which was calculated by integrating the spectral power density over  $1/f$  bandwidth for different gate voltages, was significantly lower than that reported for piezoresistive based microcantilever based sensors (2.7  $\mu\text{V}$ ) (25). Given that MOSFET current sensitivity was around 0.1 to 0.2 mA/nm of cantilever deflection, low detection

limits can be readily achieved with large S/N ratio. The noise density could likely be further reduced in subsequent generation of these devices by standard processing steps, involving optimization of doping concentration and minimizing the interface traps.

### Surface Immobilization of Receptors

For biomolecular binding experiments, the MOSFET-embedded microcantilevers were cleaned sequentially in acetone, isopropanol-2, and methanol for 10 min each, followed by UV-cleaning for 25 min, and functionalized with DTSSP ([3,3'-Dithiobis(sulfosuccinimidylpropionate)], Pierce Chemical Company), a linker molecule involved in immobilizing streptavidin and antibodies to the gold-coated microcantilever surface. Streptavidin (Pierce) was subsequently immobilized on the microcantilever surface by incubating overnight in a 10  $\mu\text{g/ml}$  streptavidin solution prepared with phosphate buffered saline (PBS, pH = 7.4). This immobilization method provides a tight streptavidin layer with uniform density on gold for efficient binding of biotin. All of the non-specific binding sites were blocked with bovine serum albumin (BSA). For detection experiments, the functionalized microcantilevers were exposed to 100  $\text{fg/ml}$ , 100  $\text{pg/ml}$ , and 100  $\text{ng/ml}$  of target biotin in PBS.

### Electronic Signature of Microcantilever Binding

MOSFET transistors were passivated with silicon nitride thin coating (30 nm) and electrical contacts were isolated for the binding measurements in the fluidic environment. The measured  $I_D$  versus  $V_{DS}$  characteristics for n-MOSFET-embedded transistor, at  $V_G=5\text{V}$ , shows a negligible change in  $I_D$  (Figure 27A) when the streptavidin immobilized gold microcantilevers are immersed in PBS.

Microcantilever bending as a result of streptavidin-biotin binding leads to decreases in  $I_D$  as the concentration of biotin increases from 100  $\text{fg/ml}$  to 100  $\text{ng/ml}$ . No drain current change was seen in  $\text{SiN}_x$  cantilevers with biotin, where no binding events occurred.

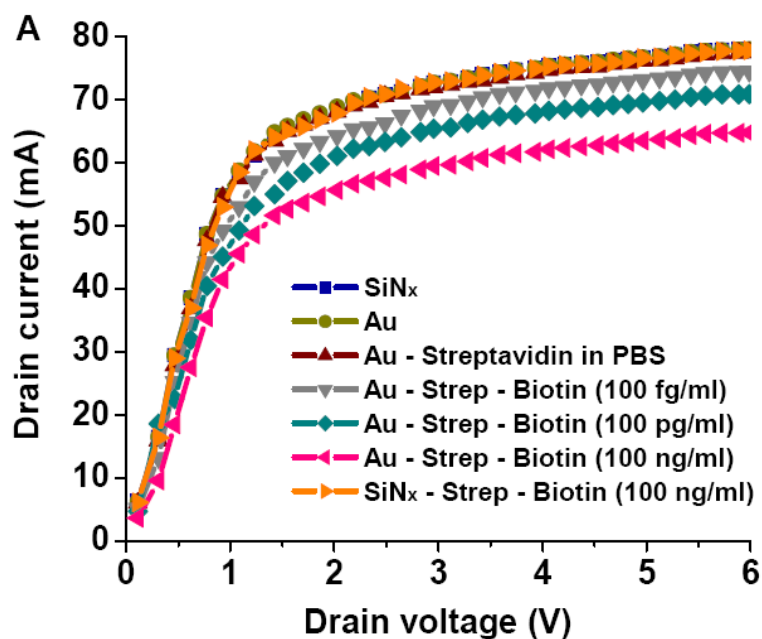


Figure 27A. MOSFET characteristics for Streptavidin-Biotin binding

Similar experiments were performed for detection of goat antibodies (secondary IgG) by rabbit antibodies (primary immunoglobulin G, IgG) with the embedded MOSFET. After the cleaning procedure, the MOSFET-embedded microcantilevers were first functionalized with DTSSP as a linker, and incubated overnight in 0.1 mg/ml rabbit anti-goat IgG (Pierce Chemical Company) prepared in PBS for immobilization. BSA was again used as an agent to block non-specific binding sites. The functionalized microcantilevers were exposed to 0.1mg/ml of goat anti-rabbit IgG in PBS for binding experiments.

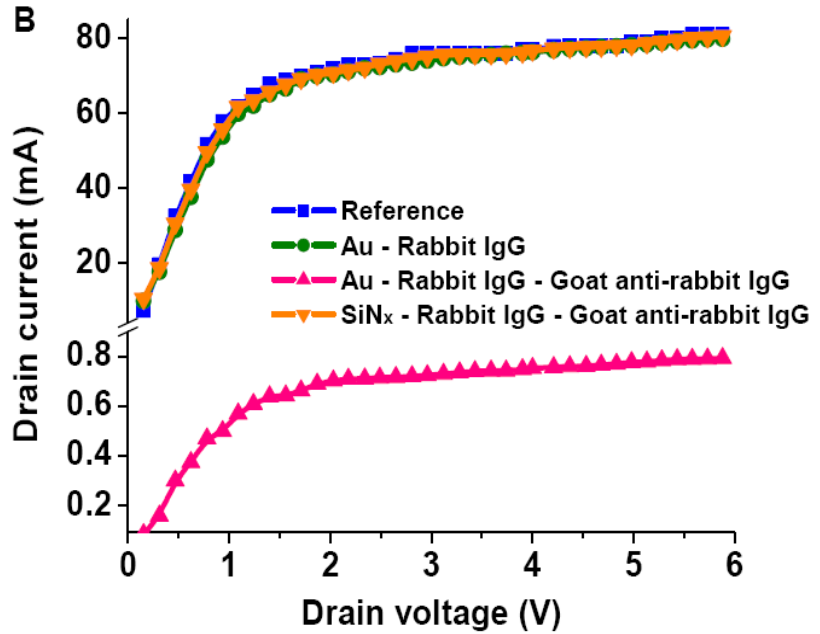


Figure 27B.  $I_D$  versus  $V_{DS}$  characteristics.

The measured  $I_D$  versus  $V_{DS}$  characteristics  $V_G = 5$  V (Figure 27B) again shows no change in the drain current when  $SiN_x$  and rabbit IgG coated cantilevers are immersed in PBS. When 0.1 mg/ml of goat anti-rabbit IgG was introduced, an almost two orders of magnitude change in  $I_D$  was observed, indicative of microcantilever bending as a result of antibody-secondary antibody binding. The  $SiN_x$  reference cantilever remained the same after injecting the target.

Thus, a novel label- and optics-free detection platform for biomolecular binding was developed. It involves high sensitivity detection of cantilever bending via embedded MOSFET drain current measurements. The MOSFET detection method offers a number of advantages over traditional piezoresistive or capacitive sensor elements because of its small size, high sensitivity, and simple direct current measurement compared to the complex piezoresistive measurements, as well as its full and seamless compatibility with direct monolithic integration with application-specific integrated circuits.

Moreover, small channel lengths of MOSFET devices provide more localized stress measurements. MOSFET-embedded microcantilever detection should allow for massively parallel on-chip signal sensing, multiplexing and remote-addressability via on-chip integration of RF (radio frequency) elements as well as photovoltaics for local power supply (Figure 28).

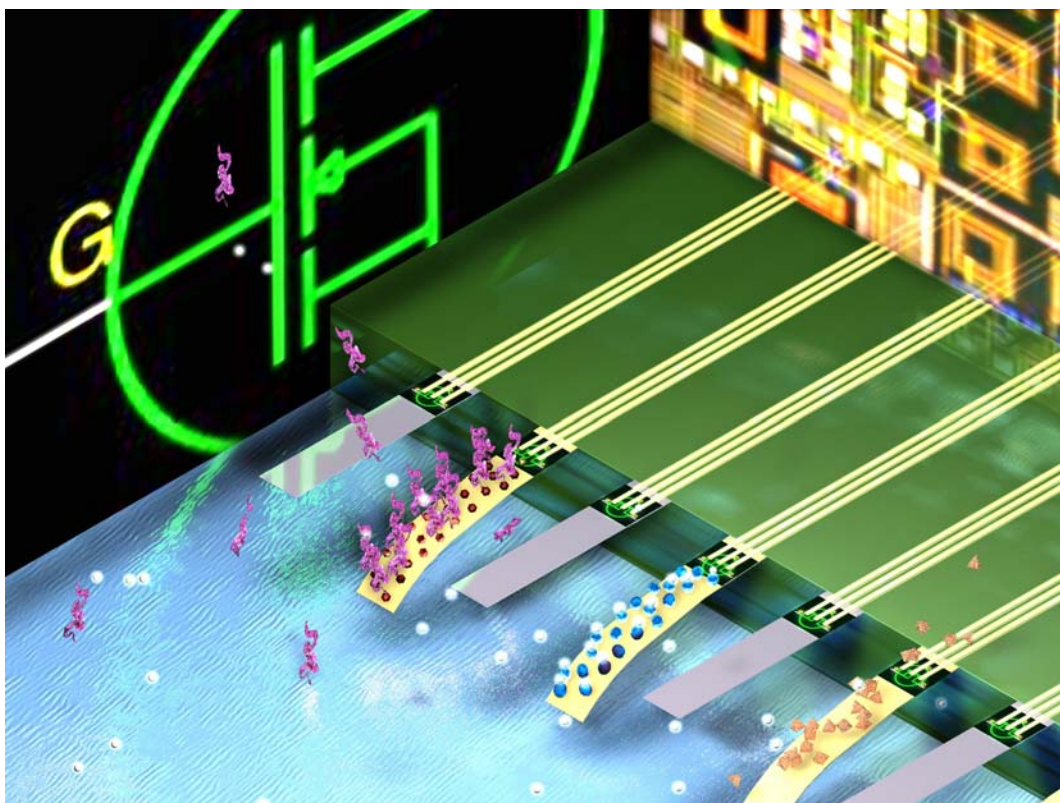


Figure 28. Schematic illustration of potential of MOSFET-embedded microcantilever array for parallel and multiplexed biomolecular detection

#### 4.0 Taking Lessons from T Lymphocyte Biology to Revolutionize Detector Design

T lymphocytes are the orchestrators of the adaptive immune response to pathogen infection. They detect the protein component of antigens that have invaded cells. Specialized cells called antigen presenting cells (APCs) display molecular signatures of the pathogen's proteins. Specifically, peptides (p) derived from pathogenic proteins bound to protein products of the major histocompatibility gene complex (MHC) are displayed on the surface of APCs. The T cell receptor (TCR) on the surface of T cells can potentially bind these pMHC molecules. The surface of the APC also displays abundant pMHC molecules where the peptide was derived from endogenous (or self) proteins. TCR can also bind to self pMHC, albeit weakly. Recent experiments carried out by one of our team members (Mark Davis, Stanford Univ.) showed that T cells can detect as few as ten stimulatory pMHC molecules in a sea of 30,000 endogenous ligands<sup>17</sup>. This extraordinary sensitivity to antigen is not accompanied by frequent spurious activation events in the absence of stimulatory (agonist) pMHC molecules. Recent theoretical work carried out as a collaboration between team members (Arup Chakraborty, UC Berkeley, and Mark Davis) has shed light on the molecular mechanisms that enable sensitive and selective detection of antigen by T cells. The goal of this seed project was to examine whether this understanding can be harnessed to design pathogen detectors that can mimic T cells in their ability to detect pathogens. Toward this end, the main goal of this project was to examine whether the APC could be replaced by a synthetic surface and yet maintain the sensitivity and

selectivity noted above. Specifically, pMHC molecules presented on supported lipid bilayers were examined to determine whether or not they can be detected sensitively and selectively by T cells. Some theoretical work exploring the signaling pathways of T cells was also pursued. The accomplishments for this aspect of the project can be summarized as follows:

1. Mixtures of pMHC molecules presented by supported lipid bilayers were detected sensitively as measured by a gross assay (immunological synapse formation).
2. Single molecule imaging methods were used to demonstrate the same as above at the single molecule level.
3. Computer simulations were conducted to examine how crowding agents inside the T cell can influence signaling, with a view toward exploring how signaling components put in a synthetic vesicle might work in the absence of crowding agents.

Below, each of these accomplishments are briefly described.

#### **Small amounts of stimulatory pMHC molecules presented on synthetic surfaces stimulate synapse formation**

Mixtures of agonist and endogenous pMHC molecules on a supported lipid bilayer were presented using methods developed by one of our team members (Michael Dustin, NYU School of Medicine) that have been described in detail previously<sup>18</sup>. T cells were then placed on top of these supported lipid bilayers, and using video microscopy, determined whether or not they were able to detect small amounts of agonists. When T cells are robustly stimulated, they form an immunological synapse<sup>18</sup>. This is a recognition motif that consists of a spatially organized collection of membrane proteins. The TCR and pMHC molecules form a tight central cluster surrounded by a peripheral ring of adhesion molecules.

Figure 29 shows that these experiments demonstrated that when a supported lipid bilayer is loaded with as little as 0.001 % agonist pMHC (the rest being a null pMHC

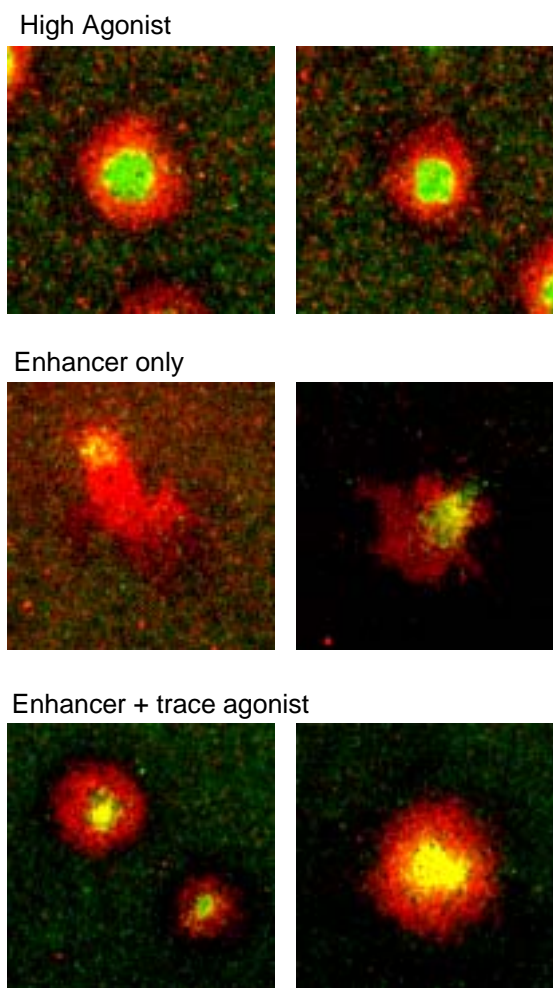


Figure 29. The synapse, a marker of robust stimulation, forms when a large amount of agonist is used and for a mixture of a small amount of agonist with null pMHC (enhancer). The enhancer, by itself, does not stimulate synapse formation.



mimic of endogenous pMHC), the T cell forms a robust immunological synapse. This indicates that, at least in gross assays, T cells are stimulated by minute amounts of agonists in a sea of non-stimulatory pMHC molecules.

### Single molecule detection of pMHC molecules on supported lipid bilayers and assays of calcium flux

The assay above only provides a gross estimate of sensitivity. Therefore, a single molecule imaging methods developed in the laboratory of our team member (Mark Davis) which has been described in detail previously<sup>17</sup> was used to examine T cell signaling at short times upon interaction with supported lipid bilayers containing mixtures of agonist and endogenous ligands. An early report of T cell signaling (calcium flux) was studied because this indicates whether or not detection would be fast.

As shown in Figure 30, preliminary results suggest that approximately 3 molecules of an agonist pMHC molecule presented on a supported lipid bilayer can be detected rapidly as determined by fluorescence imaging of calcium flux.

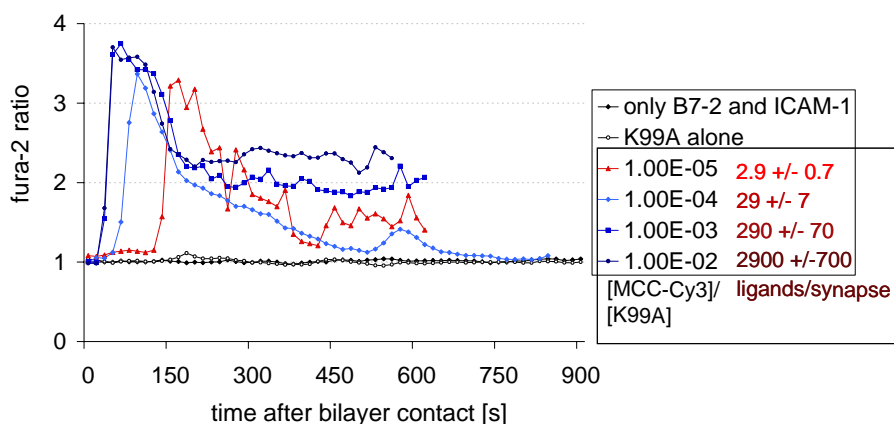


Figure 30. Single molecule imaging shows that roughly 3 molecules of an agonist pMHC displayed on a supported lipid bilayer along with a “sea” of endogenous ligands can be detected.

### The effects of molecular crowding on the T cell signaling pathway

As mentioned above, the ultimate goal of a full project would include creating a detector where even the T cell is replaced by a vesicle containing the minimal number of signaling components. Toward this end, we wanted to explore how the many inert macromolecules in the T cell influence signaling. We employed a Monte-Carlo algorithm to simulate a simplified version of the T cell signaling pathway. We studied situations where signaling is fast compared to the time scale in which the crowding agents move as well as situations where the inverse is true.

The main findings can be summarized as follows. If signal transduction occurs on timescales that are slow compared to the motility of the molecules and organelles that constitute the crowding elements, the effects of crowding are qualitatively the same as in a homogeneous 3-dimensional

medium<sup>19</sup>. In contrast, if signal transduction occurs on a timescale that is much faster than the time over which the crowding elements move, the effects of varying the extent of crowding are very different when reactions occur both in 2 and 3-dimensional space. For fast signaling, crowding agents attenuate signaling and never enhances signaling. In contrast, slow signaling cascades can be both enhanced and attenuated by crowding agents. These results were reported in detail in a publication in the *J. Physical Chemistry*<sup>20</sup>. The basic message from these studies is that the absence of crowding elements will not be strongly influence signaling and sensitivity characteristic of T cells.

## 5.0 Summary

This effort's accomplishments can be summarized as follows: 1.) Novel computational tools that can guide the design of biomolecular nanomechanical systems were developed. 2.) These tools, in close synergy with experiments, have been applied to develop prototype devices using both optical and electronic detection that are being considered for commercialization. 3.) The possibility that lessons from T cell biology could be harnessed to create novel pathogen detectors were explored setting the stage for future research opportunity.

## 6.0 References

1. J. Fritz, M. K. Baller, H. P. Lang, H. Rothuizen, P. Vettiger, E. Meyer, H. J. Güntherodt, C. Gerber, J. K. Gimzewski, Translating biomolecular recognition into nanomechanics. *Science*, vol. 288, pp. 316-318 (2000).
2. G. Wu, H. Ji, K. Hansen, T. Thundat, R. Datar, R. Cote, M. F. Hagan, A.K. Chakraborty, A. Majumdar, Origin of nanomechanical cantilever motion generated from biomolecular interactions. *Proceedings of National Academy of Science*, vol. 98, pp. 1560-1564 (2001).
3. G. Wu, R. Datar, K. Hansen, T. Thundat, R. Cote, A. Majumdar, Bioassay of prostate specific antigen (PSA) using microcantilevers. *Nature Biotechnology*, vol. 19, pp. 856-860 (2001).
4. Hagan, A. Majumdar, A. Chakraborty, "Nanomechanical Forces Generated by Surface-Grafted DNA," *Journal of Physical Chemistry B*, Vol. 106, pp. 10163-10173 (2002).
5. Dellago, C., Geissler, P., Chandler, D, Bolhuis, P, "Transition path sampling: Throwing ropes over rough mountain passes, in the dark," *Annual Reviews of Physical Chemistry*, 53: 291-318 (2002).
6. M. Hagan, A.R. Dinner, D. Chandler, A.K. Chakraborty, "Atomistic Simulation of Kinetic Pathways for DNA Unbinding and Hybridization," *Proc. Natl. Acad. Sci.*, 100, 13922 (2003).
7. A.W. Peterson, L.K. Wolf, R.M. Georgiadis, "Hybridization of mismatched or partially matched DNA at surfaces," *J. Am. Chem. Soc.*, 124, 14601 (2002).
8. M. Hagan, A.K. Chakraborty, "Hybridization Dynamics of Surface Immobilized DNA", *J. Chem. Phys.*, Vol. 120, pp 4958-4968 (2004).
9. J. C. Stachowiak, M. Yue, K. Castelino, N. Lacevic, A. Chakraborty, A. Majumdar, "Chemomechanics of Surface Stresses Induced by Biomolecular Reactions," *Langmuir*, Vol. 22, pp. 263-268 (2006).

10. M. Yue, J. C. Stachowiak, A. Majumdar, "Cantilever arrays for multiplexed mechanical analysis of biomolecular reactions," *Molecular and Cellular Biomechanics*, Vol. 1, pp. 211-220 (2004).
11. M. Yue, H. Lin, D. E. Dedrick, S. Satyanarayana, A. Majumdar, A. S. Bedekar, J. W. Jenkins, S. Sundaram, "A 2-D microcantilever array for multiplexed biomolecular analysis," *J. Microelectromechanical Systems*, Vol. 13, pp. 290-299 (2004).
12. K. Castelino, B. Kannan, A. Majumdar, "Characterization of grafting density and binding efficiency of DNA and proteins on gold films: Applications to Surface-Stress Biosensors," *Langmuir*, Vol. 21, pp. 1956-1961 (2005).
13. M. Yue, *Multiplexed Label-Free Bioassays Using Nanomechanics and Nanofluidics*, PhD Thesis, Department of Mechanical Engineering, University of California, Berkeley (2005).
14. S. Satyanarayana, D. T. McCormick, A. Majumdar, "Parylene Micro Membrane Capacitive Sensor Array for Chemical and Biological Sensing," *Sensors and Actuators B* (in press).
15. S. Satyanarayana, Surface Stress and Capacitive MEMS Sensor Arrays for Chemical and Biological Sensing, PhD Thesis, Department of Mechanical Engineering, University of California, Berkeley (2005).
16. S. Satyanarayana, R. Karnik, A. Majumdar, "Stamp and Stick Room Temperature Bonding Technique for Microdevices," *J. Microelectromechanical Systems*, Vol. 14, pp. 392-399 (2005).
17. Irvine, D. J., Purbhoo, M. A., Krogsgaard, M., and Davis, M. M., "Direct observation of ligand recognition by T cells," *Nature* 419, 845-849 (2002).
18. Grakoui, A., Bromley, S. K., Sumen, C., Davis, M. M., Shaw, A. S., Allen, P. M., and Dustin, M. L., "The immunological synapse: a molecular machine controlling T cell activation," *Science* 285, 221-227 (1999).
19. Schnell, S., Turner, T.E., "Reaction kinetics in intracellular environments with macromolecular crowding: simulations and rate laws," *Progress in Biophysics and Molecular Biology* 85, 235-260 (2004).
20. Eide, J. and Chakraborty, A.K., "Effects of quenched and annealed macromolecular crowding elements on a simple model for signaling in T lymphocytes," *J. Phys. Chem.* 110, 2318-2324 (2006).

## 7.0 Bibliography

1. M. Hagan, A. Majumdar, A. Chakraborty, "Nanomechanical Forces Generated by Surface-Grafted DNA," *Journal of Physical Chemistry B*, Vol. 106, pp. 10163-10173 (2002).
2. M. Hagan, A.R. Dinner, D. Chandler, A.K. Chakraborty, *Proc. Natl. Acad. Sci. (USA)*, (24): 13922-13927 (2003).
3. M. Yue, H. Lin, D. E. Dedrick, S. Satyanarayana, A. Majumdar, A. S. Bedekar, J. W. Jenkins, S. Sundaram, "A 2-D microcantilever array for multiplexed biomolecular analysis," *J. Microelectromechanical Systems*, Vol. 13, pp. 290-299 (2004).
4. M. Yue, J. C. Stachowiak, A. Majumdar, "Cantilever arrays for multiplexed mechanical analysis of biomolecular reactions," *Mechanics and Chemistry of Biosystems*, Vol. 1, pp. 211-220 (2004).
5. M. Hagan, A.K. Chakraborty, "Hybridization Dynamics of Surface Immobilized DNA", *J. Chem. Phys.*, Vol. 120, pp 4958-4968 (2004).
6. G.S. Shekhawat, S. Tark and V.P. Dravid, MOSFET-Embedded Microcantilevers for Measuring Deflections in Biomolecular Sensors", *Science*, Vol. 310. No. 5745, 89 (2005).



7. S. Satyanarayana, R. Karnik, A. Majumdar, "Stamp and Stick Room Temperature Bonding Technique for Microdevices," *J. Microelectromechanical Systems*, Vol. 14, pp. 392-399 (2005).
8. K. Castelino, B. Kannan, A. Majumdar, "Characterization of grafting density and binding efficiency of DNA and proteins on gold films: Applications to Surface-Stress Biosensors," *Langmuir*, Vol. 21, pp. 1956-1961 (2005).
9. B. Kannan, R. P. Kulkarni, S. Satyanarayana, K. Castelino, A. Majumdar, "Lithography-based Patterning of Functional Molecules on Surfaces for Highly Specific and Programmed Assembly of Nanostructures," *JVST-A*, Vol. 23, pp. 1364-1370 (2005).
10. J. C. Stachowiak, M. Yue, K. Castelino, N. Lacevic, A. Chakraborty, A. Majumdar, "Chemomechanics of Surface Stresses Induced by Biomolecular Reactions," *Langmuir*, Vol. 22, pp. 263-268 (2006).
11. S. Satyanarayana, D. T. McCormick, A. Majumdar, "Parylene Micro Membrane Capacitive Sensor Array for Chemical and Biological Sensing," *Sensors and Actuators B* (in press).
12. G.S. Shekhawat, S. Tark, Vinayak P. Dravid, K. Hansen, T. Thundat, "Bioassays of CRP and  $\beta$ -hCG-specific Antigens with MOSFET-embedded Microcantilevers", in-preparation, 2006.

## Appendix

### Patents & Disclosures

1. Patent Application 20020102743, "Apparatus and method for visually identifying micro-forces with a palette of cantilever array blocks," A. Majumdar et al., Filed February 13, 2002.
2. "System and Method for Multiplexed Biomolecular Analysis," A. Majumdar et al., Filed Nov. 15, 2002.
3. "Composite Sensor Membrane," A. Majumdar, S. Satyanarayana, M. Yue, Filed April 21, 2003.
4. "Stamp-and-Stick Chip Bonding," A. Majumdar, S. Satyanarayana, R. Karnik, Provisional patent filed, June '04.
5. G. Shekhawat and Vinayak P. Dravid, "Electronic Detection of Mechanical Perturbation", NU disclosure # 23072, patent filed, August 2005.
6. Method for high sensitivity electronic detection of biochemicals using MOSFET-embedded microcantilevers, filed for patent, Fall 2005

### Personnel Trained:

Min Yue, PhD student in Mechanical Engineering at UC Berkeley

Srinath Satyanarayana, PhD student in Mechanical Engineering at UC Berkeley

Kenneth Castelino, PhD student in Mechanical Engineering at UC Berkeley

Balaji Kannan, PhD student in Mechanical Engineering at UC Berkeley (supported through a grant from the College of Engineering)

Jeanne Stachowiak, MS student in Mechanical Engineering at UC Berkeley (supported through a fellowship).

M.F. Hagan, PhD student in chemical engineering at UC Berkeley

A.R. Dinner, Postdoctoral Fellow at UC Berkeley (supported through a fellowship)  
N. Lacevic, Postdoctoral Fellow at UC Berkeley